# Journal of Materials Chemistry A

Accepted Manuscript






ROYAL SOCIETY OF CHEMISTRY

www.rsc.org/materialsA

Journal Name

COMMUNICATION

# Preparation of $Sn@SnO_2@C@MoS_2$ composite as high-performance anode material for lithium-ion batteries

Received 00th January 20xx,
Accepted 00th January 20xx

DOI: 10.1039/x0xx00000x

www.rsc.org/

Youguo Huang,[a] Qichang Pan,[a] Hongqiang Wang,*[a] Cheng Ji,[a] Xianming Wu,[b] Zeqiang He[b] and Qingyu Li*[c]

**A new type of $Sn@SnO_2@C@MoS_2$ composite, composed of $Sn@SnO_2@C$ nanosheets and decorated with $MoS_2$, which exhibits significantly improved electrochimical performance. Contributing to excellent long-term cycling stability (841 mAh/g at 1.0 A/g after 400 cycles) and superior high-rate capability (458.3 mAh/g at 10.0 A/g) due to the strong synergistic effect between the $MoS_2$ and Sn@C nanosheets.**

Lithium ion batteries have been widely used as a power supply for hybrid electric vehicles, electric vehicles and portable electronic devices because of their high energy density and long cycle life.[1,2] Graphite, the commercial anode material is far from meeting the demand for high energy density due to its low theoretical capacity (372 mAh/g). Recently, Sn-based materials have been considered as one of the most promising alternative anode materials for next-generation lithium-ion batteries due to its high theoretical capacity and well-suited discharge potential.[3] However, the practical application of Sn-based materials have been greatly hampered by its pulverization problem caused by the huge volume change during the lithiation/delithiation processes, resulting in poor cycle performance and rate capability.[4]

In order to improve the electrochemical performances of Sn-based anode materials, significant efforts have been made to alleviate these problems. One approach involves the doping of inactive phase such as Cu, Ni and Co to buffer the volume variation of Sn-based materials.[5-7] Another effective approach is designed for Sn-based nanocomposite such as Sn-carbonaceous nanocomposites,[8,9] Sn@CNT nanocomposites,[10] Sn/graphene nanocomposites[11] and other Sn-based nanocomposites.[12,13] Among these nanocomposites, Sn-carbonaceous nanocomposites have shown inherent and great potential for further development. These carbon matrices can not only provide spaces to buffer the mechanical stress induced by the volume change of the Sn-based materials, but also enhance the electric conductivity, resulting in significant improved cycling performance.

Recently, layer-structured molybdenum disulfide ($MoS_2$) has recently attracted much attention due to its high reversible capacity.[14,15] On one hand, the structure of $MoS_2$ is analogous to that of graphite, in which the S-Mo-S layers are held together by van der Waals forces.[16] With such atomic arrangement, lithium ions can freely move within the space between adjacent layers and interact with $MoS_2$ with low volume expansion and contraction. On the other hand, $MoS_2$ have a high mechanical strength with a Young's modulus of 230 GPa. Such strong methanical behavior helps $MoS_2$ nanosheets to accommodate the severe structural deformation of the other anode materials incorporated during the charge and discharge process.[17]

Here, we report a novel $Sn@SnO_2@C@MoS_2$ nanocomposite for lithium ion batteries anode materials. Fig.1 describes the fabrication process. Firstly, Sn@C nanosheets were synthesized by a facile ball milling using NaCl as the template. In this step consists in dissolving NaCl, $SnCl_2$, $Na_3C_6H_5O_7$ in distilled water by ball milling, which was subsequently dried and then calcined at 700 °C under Ar atmosphere. During the drying process, the NaCl particles uniformly coated with $SnO_2$-$Na_3C_6H_5O_7$ film, upon heating the composite at high temperature under Ar, the $SnO_2$ was reduced to Sn nanoparticles and $Na_3C_6H_5O_7$ as carbon source

[a]School of Chemistry and Pharmaceutical Sciences, Guangxi Normal University, Guilin, 541004, China.E-mail: whq74@126.com;Fax: +86-0773-5858562

[b]The Collaborative Innovation Center of Manganese-Zinc-Vanadium Industrial Technology (the 2011 Plan of Hunan Province), Jishou,Hunan,416000

[c]Guangxi Key Laboratory of Low Carbon Energy Materials, Guangxi Normal University, Guilin, 541004, China. E-mail: liqingyu62@126.com.

forming to carbon nanosheets.[18] Subsequently, the obtained Sn@C nanosheets were used as substrates for the decoration of $MoS_2$ via hydrothermal method. In the final product of Sn@$SnO_2$@C nanosheets decorated by $MoS_2$, the $MoS_2$ and carbon can accommodate the large volume changes of Sn@$SnO_2$ during charge and discharge process. Additionally, the $MoS_2$ also can facilitates Li intercalation/extraction.[19] When the composite evaluated as an anode materials for lithium ion batteries, exhibited remarkably improved electrochemical performance as high as 841.0 mAh/g after 400 cycles at current density of 1.0 A/g.

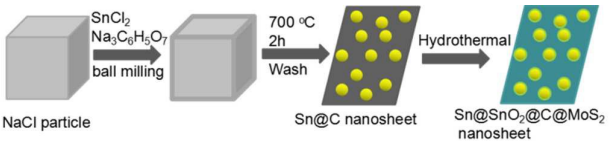


Fig.1 Schematic illustration of the fabrication process

The crystalline structure of the Sn@C composite and Sn@$SnO_2$@C@$MoS_2$ composite were investigated by X-ray diffraction (XRD) are shown in Fig. S1. For the Sn@C composite shown at the figure, all the observed strong and apparent diffraction peaks can be indexed well to Sn (JCPDS no. 04-0673), the sharpness of the diffraction peaks indicates that the tin phase in the products is highly crystallized.[20] As for Sn@$SnO_2$@C@$MoS_2$ composite, it can clearly see from Fig. S1 that all intensive peaks can be well indexed to pure rutile $SnO_2$ (JCPDS card no. 41-1445) and crystalline tin ((JCPDS card no. 04-0673). It is suggested that some crystalline tin transformed into $SnO_2$ after hydrothermal process. In addition, it is also found some slight peaks can be assigned to the crystalline planes of hexagonal $MoS_2$ phase (JCPDS card no. 37-1492). Especially, the distinct peak at 14.2° characteristic of the (002) crystalline plane for MoS2 suggests the ordered stacking of S-Mo-S layers.[21] In addition to, no diffraction peaks corresponding to crystalline carbon were observed in the composites, indicating that the carbon remained amorphous.

Raman spectroscopy was further utilized to characterize the composition of the obtained the Sn@$SnO_2$@C@$MoS_2$ composite. As shown in Fig. S2, Sn@$SnO_2$@C@$MoS_2$ composite was observed two distinct peaks at the bands of 380 and 407 $cm^{-1}$, which correspond to the $E^1_{2g}$ vibration mode and $A_{1g}$ vibration mode.[21] In addition, The G-band around 1573 $cm^{-1}$ and the D-band around 1352 $cm^{-1}$ are typical bands of carbonaceous materials.[23] So all of these results further confirm that we have successfully prepared the Sn@$SnO_2$@C@$MoS_2$ composite.

The morphology and microstructure of the products were obtained using scanning electron microscope (SEM) and transmission electron microscope (TEM). The SEM images (Fig. 2A and 2C) shows that the Sn@C composite and Sn@$SnO_2$@C@$MoS_2$ composite has nanosheets-structure morphology with some nanoparticles embedded in nanosheets, and these nanoparticles with a diameter about 100 nm. However, after undergoing a hydrothermal coating reaction, the surface of the Sn@$SnO_2$@C@$MoS_2$ composite becomes much rougher than the Sn@C composite, indicating the successful growth of $MoS_2$ onto Sn@C nanosheets after hydrothermal reaction (Fig. 2B and 2D). In addition, the nanosheets-structure morphology and nanoparticles have not obviously changed after hydrothermal reaction.

Transmission electron microscope (TEM) was further employed to investigate the structure of the Sn@$SnO_2$@C@$MoS_2$ composite. The TEM image clearly (Fig. 3A) shows that tin nanoparticles coated by an interconnected carbon and $MoS_2$ porous network, as shown in Fig. 3B, it is clearly discerned that the tin

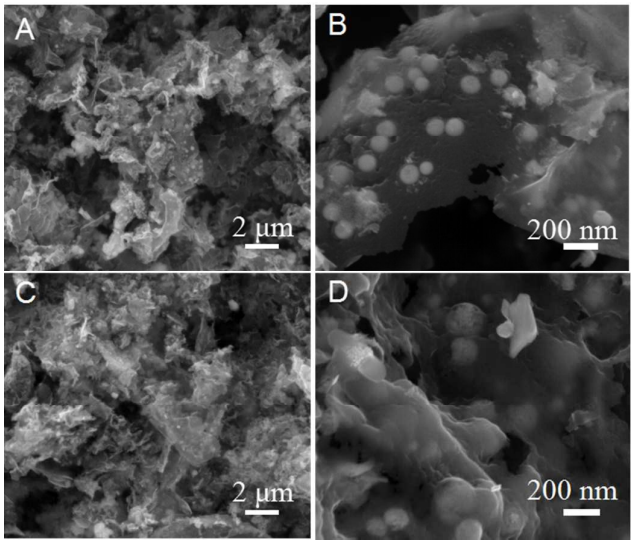


Fig.2 SEM images of (A,B) Sn@C composite and (C,D) Sn@$SnO_2$@C@$MoS_2$ composite.

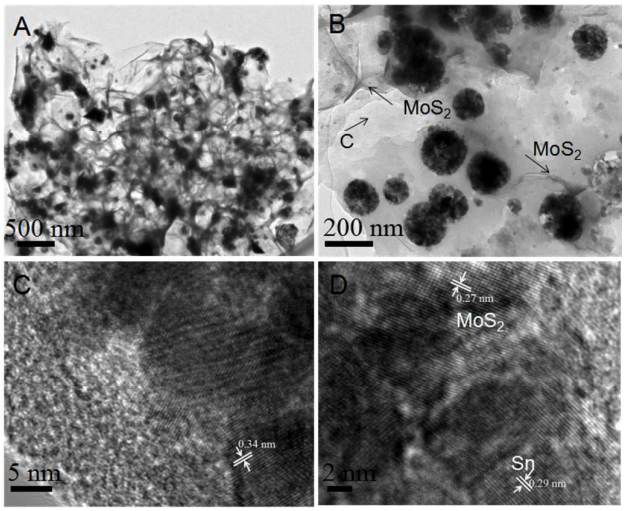


Fig. 3(A,B) TEM and (C,D) HRTEM images of the $Sn@SnO_2@C@MoS_2$ composite

nanoparticles embedded in the carbon nanosheets and then coated by $MoS_2$. Furthermore, the lattice fringe orientations in the HRTEM images (Fig. 3 C,D) demonstrate clear lattice fringes with *d*-spacings of 0.29 nm, 0.34 nm and 0.27 nm, which are in good agreement with that of the (200) plane of the Sn crystal, the (110) plane of $SnO_2$ and the (100) plane the $MoS_2$, respectively.

To gain insight into the chemical composition, thermogravimetric analysis (TGA) was carried out the Sn@C and $Sn@SnO_2@C@MoS_2$ composite, as shown in Fig. S3. On one hand, for the Sn@C composite, a weight loss observed at approximately 350 $^oC$ owing to the the sample is annealed under air to oxidize Sn to $SnO_2$ and carbon to $CO_2$, on the basis of the final weight of $SnO_2$, the Sn@C composite content of Sn is calculated to be 47.71 wt%. On the other hand, for the $Sn@SnO_2@C@MoS_2$ composite, the one continuous weight loss in the range of approximately 150-350 $^oC$ for the $Sn@SnO_2@C@MoS_2$ composite is attributed to the oxidation of $MoS_2$ to $MoO_3$, Sn to $SnO_2$ and the decomposition of amorphous carbon.[24] Based on the TGA result, the mass fraction of $Sn@SnO_2$, $MoS_2$ and C in the $Sn@SnO_2@C@MoS_2$ composite can be calculated to be around 30.3 wt%, 36.49 wt% and 33.21 wt%, respectively.

The electrochemical properties were investigated for $Sn@SnO_2@C@MoS_2$ composite as an anode for lithium-ion batteries. The composite first evaluated by cyclic voltammogram (CV) at a scan rate of 0.1 mV/s. Fig. 4 displays the CV curves for the first and second cycles of the $Sn@SnO_2@C@MoS_2$ electrode at a sweep rate of 0.1 mV s-1 within a potential window of 0.005-3.0 V. In the first cathodic scan, the peak at 0.8 V can be assigned to the reduction of $SnO_2$ to $Li_2O$/Sn as well as the formation of SEI layers, and another peak at 0.1 V is related to the formation of $Li_xSn$ alloys, and the peak at around at 0.21 V correspond to the conversion reaction process: $MoS_2 + 4Li + 4e^- \leftrightarrow Mo + 2Li_2S$ . The following anodic scan gives peaks between 0.25 V and 0.9 V may be assigned to the delithiation reaction of the $Li_xSn$ alloy, the broad anodic peak at around 1.25 V represents the partial oxidation of Sn to $SnO_x$, and the oxidation peak at around 2.3 V, which is due to the oxidation pf $Li_2S$ to S and lithium ions.[25,26]

Fig. S4 shows the first charge and discharge curves of the $Sn@SnO_2@C@MoS_2$ composite. The discharge capacity and charge capacity are 1773.3 mAh/g and 2112.2 mAh/g, respectively. The irreversible capacity loss is mainly due to SEI film formation in the initial discharge process. In addition, during the charge process, a plateau appearing at around 2.3 V is observed, which is in accordance with the previous CV curves.

During the discharge process, a plateau at around 1.8 V

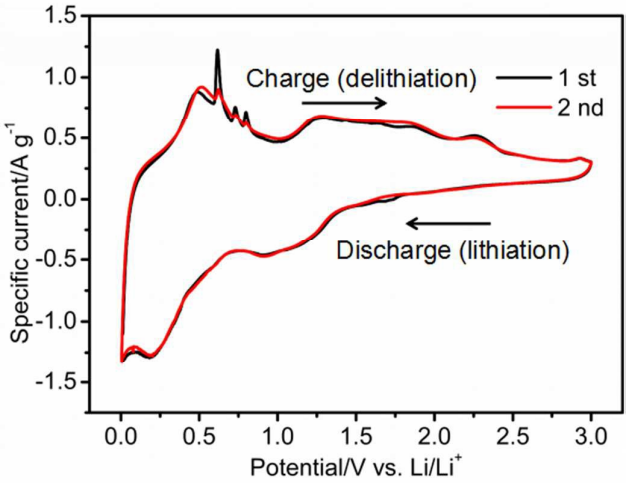


Fig. 4 Cyclic voltammogram of the $Sn@SnO_2@C@MoS_2$ composite at a scan rate of 0.1 mV $s^{-1}$.

and a gentle slope between 0.25 V and 0.9 V are observed, which is also in agreement with the above CV study.

In order to confirm that the superiority of the $Sn@SnO_2@C@MoS_2$ composite over Sn@C composite in lithium storage performance, we compare their cycle behaviours as shown in Fig. 5A. Clearly, $Sn@SnO_2@C@MoS_2$ composite delivers a capacity of 861.3 mAh/g after 100 cycles at current density of 200 mA/g. In contrast, Sn@C composite only deliver a capacity of 443.8 mAh/g after 100 cycles at the same current density. It is very obviously that the cycling performance of the $Sn@SnO_2@C@MoS_2$ composite is significantly improved compared to Sn@C composite after introduction of $MoS_2$. Therefore, the $Sn@SnO_2@C@MoS_2$ composite can significantly enhance the cyclic stability due to the strong synergistic effect between the $MoS_2$ and Sn@C nanosheets.

Furthermore, the $Sn@SnO_2@C@MoS_2$ composite also exhibits superior rate capability, as shown in Fig. 5B, delivering high reversible capacities of 1213.5 mAh/g, 1062 mAh/g, 949.9 mAh/g, 813.8 mAh/g, 633.1 mAh/g and 458.3 mAh/g when cycled at current densities of 200, 500, 1000, 2000, 5000 and 10000 mA/g. It is wroth mentioning that even after deep cycling at 10000 mA/g, the reversible capacity can return to 790.5 mAh/g when the current density is recovered to 200 mA/g, further confirming the superior rate performances of the $Sn@SnO_2@C@MoS_2$ composite. On the other hand, in order to further confirm the superior performance of the $Sn@SnO_2@C@MoS_2$ composite, the long-term cycling stability at high current density of 1.0 A/g of the $Sn@SnO_2@C@MoS_2$ composite has also been explored, and the result is shown in Fig. 5C. The discharge capacity of the $Sn@SnO_2@C@MoS_2$ composite was 841 mAh/g after 400 cycles. Such extremely high cycling capability and stability at high rate is superior

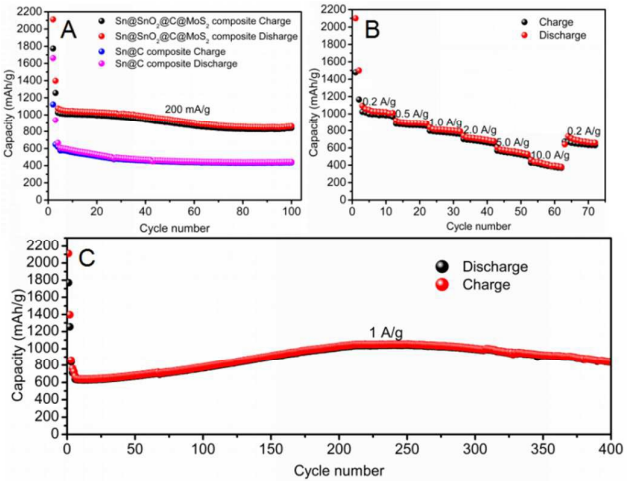


Fig. 5 (A) Cycling performance of the $Sn@SnO_2@C@MoS_2$ composite at a constant current density of 200 mA g1. (B) Rateperformance of the $Sn@SnO_2@C@MoS_2$ composite. (C) Cycling performance of the $Sn@SnO_2@C@MoS_2$ composite at a current density of 1 A $g^{-1}$.

to the previously reported Sn-based anode materials.[27,28] The enhanced capacity is attributed to the $MoS_2$ can offer a mass of active sites for hosting lithium ions, and also can greatly shorten the diffusion distance of both electrons and ions.[29,30] In addition, the composite shows a continuous increasing of capacity from 11$^{th}$ to 200$^{th}$ cycles, the enhanced capacity is attributed to more and more available sites from both $Sn@SnO_2$ and $MoS_2$ and possibly interfacial lithium storage as well as electrochemical activation of the hybrid during the cycling process. [31.32]

In order to further understand the excellent electrochemical performance, the morphology and structure changes of the $Sn@SnO_2@C@MoS_2$ composite after deep charge/discharge cycles were explored by TEM. As shown in Fig. S5A, B and C, the $Sn@SnO_2$ nanoparticles pulverized into smaller particles, but still encapsulated in the nanosheets. The high resolution TEM image in Fig. S5D demonstrated that after cycling the small pulversized Sn nanoparticles with a lattice of 0.29 nm could be seen clearly. Therefore, the TEM images of the $Sn@SnO_2@C@MoS_2$ composite after deep cycles also demonstrated that the excellent electrochemical performance.

The above results clearly confirm that the $Sn@SnO_2@C@MoS_2$ composite has superior cycle and rate performance, which can be ascribed to the synergistic effect between the $Sn@SnO_2$ nanoparticles, carbon nanosheets and $MoS_2$. First, the carbon nanosheets and $MoS_2$ encapsulated $Sn@SnO_2$ nanoparticles not only avoid the direct exposure of the electrolyte and preserve the structural and interfacial stabilization of $Sn@SnO_2$ nanoparticles but also buffer the volume expansion during the charge/discharge process. Second, the $Sn@SnO_2$ nanoparticles can off a great deal of active sites for lithium ion. Third, the $MoS_2$ nanosheets can offer a mass of active sites for hosting lithium ions and also can greatly shorten the diffusion distance of both electrons and ions.[33,34] So resulting in excellent long-term cycling stability and superior high-rate cyclability due to the strong synergistic effect between the $MoS_2$ and $Sn@SnO_2@C$ nanosheets.

## Conclusions

In summery, we have developed a facile method for the synthesis of $Sn@SnO_2@C@MoS_2$ composite for high-performance lithium ion batteries anode materials. On one hand, the carbon nanosheets and $MoS_2$ serving as matrix can buffer the volume change of the $Sn@SnO_2$ nanoparticles during the cycling process. On the other hand, $MoS_2$ can offer a mass of active sites for hosting lithium ions, and also can greatly shorten the diffusion distance of both electrons and ions, which is favorable for enhancing the high-rate cycling capacity and good coulombic efficiency. The $Sn@SnO_2@C@MoS_2$ composite delivers a reversible capacity of 458.3 mAh/g even at high current density of 10 A/g, and also deliver a capacity of 841 mAh/g after 400 cycles at current density of 1 A/g when evaluated as anode for lithium ion batteries, exhibiting a huge potential as next generation of LIB electrode materials.

## Acknowledgements

This work was supported by the National Science Foundation of China (U51364004, 51474077, 21473042, 51474110, 1401246).

## Notes and references


1.W. Xu, J. L. Wang, F. Ding, X. L. Chen, E. Nasybulin, Y. H. Zhang and J. G. Zhang, Energy Environ. Sci., 2014, **7**, 513.

2. W. W. Lee and J. M. Lee, J. Mater. Chem. A, 2014, **2**, 1589.

3. Y. C. Liu, N. Zhang, L. F Jiao, Z. L. Tao and J. Chen, Adv. Funct. Mater. , 2015, **25**, 214.

4. Z. Q. Zhu, S. W. Wang, J. Du, Q. Jin, T. R. Zhang, F. Y. Cheng and J. Chen, Nano Lett. , 2014, **14**, 153.

5. S. L. Wang, W. Z. Zhao, Y. Wang, X. Liu and L. Li, Electrochim. Acta, 2013, **109**, 46.

6. K. Zhuo, M. G. Jeong, C. H. Chung, J. Power Sources, 2013, **244**, 601.

7. J. Hassoun, G. Mulas, S. Panero and B. Scrosati, Electrochem. Commun. , 2007, **9**, 2075.

8. W. Li, R. Yang, J. Zheng, X. G. Li, Nano Energy, 2013, **2**, 1314.

9. N. Li, H. W. Song, H. Cui, G. W. Yang and C. X. Wang, J. Mater. Chem. A, 2014, **2**, 2526.

10. J. S. Zhu, D. L. Wang, L. B. Cao and T. F. Liu, J. Mater. Chem. A, 2014, **2**, 12918.

11. J. Z. Chen, L. Yang, Z. X. Zhang, S. H. Fang and S. I. Hirano, Chem. Commun., 2013, **49**, 2792.

12. H. Q, Wang, Q. C. Pan, J. Chen, Y. H. Zan, Y. G. Huang,G. H. Yang, Z.X. Yan and Q. Y. Li, New J. Chem., 2016, **40**, 1263.

13. J. Shao, Q. T. Qu, Z. M. Wan, T. Gao, Z. C. Zuo, andH. H. Zheng, ACS Appl. Mater. Interfaces , 2015, **7**, 22927.

14. T. Stephenson, Z. Li, B. Olsena and D. Mitlin, Energy Environ. Sci., 2014, **7**, 209.

15. Y. Chen, J. Lu, S. Wen, L. Lu and J. M. Xue, J. Mater. Chem. A, 2014, **2**, 17857.

16. L. Zhang, H. B. Wu, Y. Yan, X. Wang and X. Wen (David)Lou, Energy Environ. Sci., 2014, **7**, 3302.

17. Q. C. Pan, Y. G. Huang, H. Q. Wang, G. H. Yang, J. Chen, Y. H. Zan, Q. Y. Li, Electrochim. Acta , 2016, **197**, 50.

18. J. Qin, C. N. He, N. Q. Zhao and J. J. Li, ACS Nano, 8, 1728.

19. X. Li, J. Y. Zhang, R. Wang, H. Y. Huang, C. Xie, Z. H. Li, J Li and C M. Niu, Nano Lett. , 2015, **15**, 5268.

20. Y. G. Huang, Q. C. Pan, H. Q. Wang, G. H. Yang. Q. Wu and Q. Y. Li, Ceram. Int. , 2016, 42, 4586.

21. X. D. Li, W. Li, M. C. Li, H. Y. Liu and G. S. Song, J. Mater. Chem. A, 2015, 3, 2762.

22. H. H. Zhao, H. Zeng, Y. Wu, S. G. Zhang, B. Li and Y. H. Huang, J. Mater. Chem. A, 2015, **3**, 10466.

23. Y. Fang, Y. Y. Lv, R. C. Che, H. Y. Wu, X. H. Zhang, D. Gu, G. F. Zhengand D. Y. Zhao, J. Am. Chem. Soc. , 2013, **135**, 1524.

24. Q. Y. Li, Q. C. Pan, G. H. Yang, X. L. Lin, Z. X. Yan,H. Q. Wang and Y. G. Huang, J. Mater. Chem. A, 2015, **3**, 20375.

25. X. s. Zhou, Z. H. Dai, S. H. Liu, J. C. Bao Y. G. Guo, Adv. Mater. , 2014, **26**, 3943.

26. C. B. Zhu, X. K. Mu, P. A. van Aken, Y. Yu and J. C. Maier, Angew. Chem. , 2014, **126**, 2184.

27. I. Meschini, F. Nobili, M. Mancini, R. Marassi, R. Tossici, F. Croce a, J. Power Sources, 2013, 226, 241.

28. H. Q. Wang, G. H. Yang, Y. G. Huang, X. H. Zhang, Z. X. Yan, Q. Y. Li, Mater. Chem. Phys. , 2015, 167, 303.

29. D. B. Kong, H. Y. He, Q. Song, B. Wang, W. Lv, Q. H. Yang and L.J. Zhi, Energy Environ. Sci., 2014, **7**, 3320.

30. S. Hu, W. Chen, J. Zhou, F. Yin, E. Uchaker, Q. F. Zhang and G. Z. Cao, J. Mater. Chem. A, 2014, **2**, 7862.

31. Y. Chen , B. H. Song , X. S. Tang , L. Lu and J. M. Xue, Small, 2014, 10, 1536.

32. R. H. Wang,C. H. Xu,J. Sun, Y. Q. Liu,L. Gao, H. L. Yao, C. C. Lin, Nano Energy, 2014, 8, 183.

33. B. J. Guo, K. Yu, H. Fu, Q. Q. Hua, R. J. Qi, H. L. Li, H. L. Song, J. Mater. Chem. A, 2015, 3, 6392.

34. J. B. Ye, L. Ma, W. X. Chen, Y. J. Ma, F. H. Huang, C. Gao, J. Mater. Chem. A, 2015, 3, 6884.

$Sn@SnO_2@C$ nanosheets decorated with $MoS_2$ is prepared via a facile ball milling and hydrothermal method, and the $Sn@SnO_2@C@MoS_2$ composite shows high capacity and long-term cycling stability when used as anode material for lithium-ion batteries.